Worcester Polytechnic Institute

A Major Qualifying Project

SCREAM

Super-elastic Continuum Robot for Endoscopic Articulation and Manipulation

Submitted By:

Zachary Boyer, Robotics Engineering & Mechanical Engineering

Cory Brolliar, Robotics Engineering

Benjamin Mart, Robotics Engineering & Mechanical Engineering

Kevin O'Brien, Computer Science

Advised By:

Loris Fichera, Robotics Engineering & Computer Science

Greg Fischer, Robotics Engineering & Mechanical Engineering

Ken Stafford, Robotics Engineering & Mechanical Engineering

Contents

List of Figures

List of Tables

Abstract

Office-based endoscopic procedures are an increasingly attractive option for the treatment of laryngeal tumors, but their effectiveness is limited by the restricted range of motions attainable by state-of-the-art surgical instruments. In this project, we propose a new ultra-thin dexterous manipulator made of super-elastic nitinol intended to amplify a surgeon's manipulation capability during endoscopic procedures. Included with our tool is a graphical feedback system that offers intuitive visualization of the manipulator's configuration in real-time. The overarching goal of this research is to lay the groundwork for the creation of a new class of FDA-approved miniature steerable instruments for in-office laryngeal treatment.

Acknowledgements

Professors Fichera, Fischer, Stafford, WPI, Worcester, MA

Thomas L. Carroll, MD, Harvard Medical School, Brigham and Women's Voice Program, Brigham and Women's Hospital, Boston, MA

Tom Partington, Machinist, Goddard Machine Shop, WPI, Worcester, MA

Kat Crighton, Robotics Engineering, WPI, Worcester, MA

Colleen Shaver, Robotics Resource Center, WPI, Worcester, MA

Alex Chiluisa, Ph.D. Student, COMET Lab, WPI, Worcester, MA

Karim Tarabein, Ph.D. Student, COMET Lab, WPI, Worcester, MA

The Cancer Genome Atlas Program (TCGA), `cancergenome.nih.gov`

1 Introduction

Laryngeal lesions, both benign and malignant, can cause speech impairment by interrupting the normal physiologic vibration of the vocal folds. Benign lesions alone (e.g. polyps, nodules or cysts) are prevalent in the general population with an estimated 3% of individuals affected [1]. Surgical removal of laryngeal lesions is normally performed in the operating room under general anesthesia [2], but new treatment protocols are currently being investigated to treat laryngeal disease in an office setting [3]. The main technological advancement that enabled the development of these new protocols is the progressive miniaturization of flexible chip-tip camera endoscopes, which are now commercially available in diameters suitable for trans-nasal use in conscious patients, as illustrated in Figure 1(a). These endoscopes are equipped with a working channel which can be used to deploy surgical instrumentation (e.g. a pair of miniaturized forceps or a laser fiber). The advantages of performing laryngeal surgery in the office are manifold: office procedures eliminate the need for general anesthesia (and its associated risks) [3], cost significantly less [4, 5] and involve a much shorter procedural time [5] when compared to procedures in the operating room.

Despite these benefits, in-office laryngeal surgery still presents several technical limita-

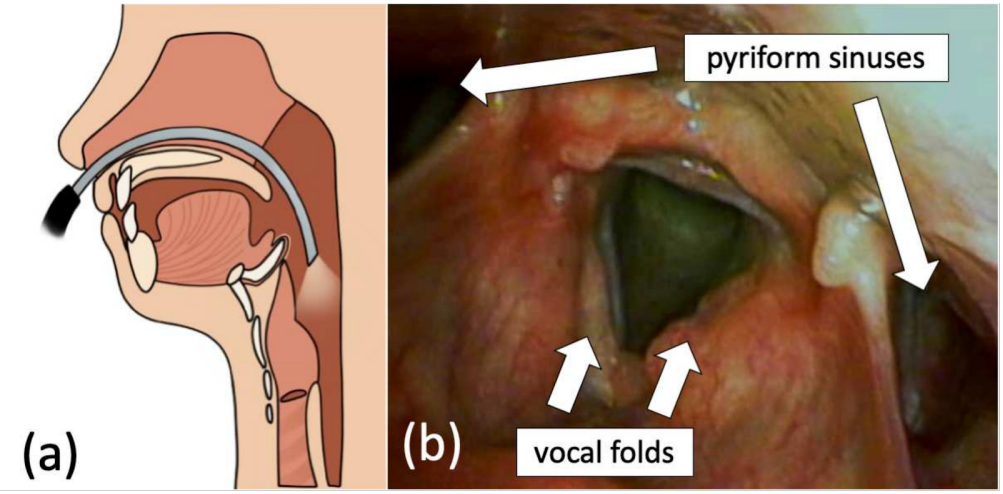

Figure 1: (a)Trans-nasal endoscopy of the larynx; (b)Intra-operative view, with pathology appearing on the vocal folds

tions which hinder routine application. One of the major challenges is represented by the restricted range of maneuvers attainable with available instrumentation [3, 6, 7, 8]; trans-nasal endoscopes can be made to bend in different directions, but the small diameter of the working channel (typically ≤ 2 millimeters (mm)) does not permit the passage of instruments equipped with articulation mechanisms. Lack of instrument articulation creates two practical problems: (i) it makes it impossible to manipulate tissue without bending the endoscope—i.e. without constantly changing the field of vision—which makes manipulation non-intuitive and often creates inadequate exposures of the surgical field [7]; (ii) it precludes access to those anatomical locations that cannot be reached in a linear path [7, 6]. Relevant examples include the under-surface of the vocal folds and the pyriform sinuses (shown in Figure 1(b)), a pair of cavities located lateral to and posterior to the voice box [9].

Aiming to overcome the issues outlined above, in this paper we propose exploring the creation of new surgical instrumentation for office-based laryngeal surgery. We envision the creation of miniaturized steerable tools that can be deployed through the operating channel of a trans-nasal endoscope. The tools will be equipped with distal bending in order to amplify a surgeon's manipulation ability inside the larynx.

1.1 Clinical Significance

To better illustrate the significance of this work, in this section we describe a specific disease state which we believe would immensely benefit from the instruments we propose. Recurrent Respiratory Papillomatosis (RRP) is a pathological condition of the human larynx characterized by the recurrent growth of multiple benign tumors (papillomas). According to the RRP Foundation, there are about 20,000 active cases of RRP in the United States today [10]. Symptoms of RRP include hoarseness and, in more severe cases, shortness of breath secondary to the occlusion of the airway caused by the growth of the tumors. Although benign, if untreated, these tumors can quickly progress down into the respiratory tract, spread to the trachea and, in some cases, spread to the lungs [10].

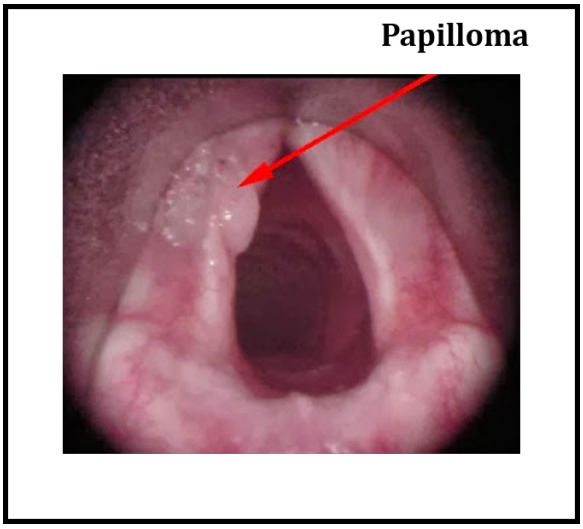

Figure 2: Recurrent Respiratory Papillomatosis manifesting on vocal folds

Modern strategies for the management of RRP involve surgical treatment in the operating room. Historically, physicans used non-heated instruments to remove papillomas from the airway. Other techniques were later introduced which involve the use of lasers to cauterize diseased tissue in-situ [11]. Because these operations are performed under general anesthesia, they are associated with a number of possible clinical complications [12]. Due to the recurrent nature of this condition, it is not uncommon for an RRP patient to require numerous surgeries per year to surveil and control the spread of the disease, resulting in an average of 100 surgeries in a patient's lifetime [12]. It is estimated that the total lifetime cost of treatment for an RRP patient in the United States is in excess of $200,000 [13].

Completing procedures in the office rather than the operating room reduces the cost for the patient. As described earlier, current medical device limitations significantly impact the treatment of laryngeal diseases such as RRP. When perfect alignment between the lesion, endoscope, and laser waveguide is not achievable, such as in the case of a lesion on the underside of the vocal folds, current procedures dictate that more substantial treatment may be necessary (i.e. open surgery). Such operations may cost patients upwards of $5000 more than an in-office procedure would, thus putting a substantial financial burden on the patient and their family [4].

1.2 Paper Outline

The outline of this paper is as follows:

Section 2 presents a study aimed to establish kinematic requirements for instrument operation in the larynx. It provides a simulation framework for establishing these requirements. It also describes in detail the design of the instrument and its fabrication. Finally, it concludes with an overview of sensors and visualization tools.

Section 3 presents benchmark validations of the instrument's capabilities and an in vitro test of the instrument.

Section 4 concludes the paper and provides opportunities for further work.

2 Materials and Methods

Creating steering instruments at the scale required for our application is not straightforward, as articulation mechanisms based on traditional linkages (e.g. ball/universal joints, cables and pulleys) can only be miniaturized to a certain extent [14]. We propose tackling these challenges by exploring the use of miniaturized tube-like continuum bending mechanisms. Curved bending sections can be realized in the body of a thin tube via the creation of notches and the attachment of a pull-write at the tip [15]. Different tube materials have been demonstrated in the literature, including super-elastic Nickel-Titanium (NiTi) [15, 16] and polyether ether ketone (PEEK) [17]. These bending mechanisms present two characteristics that make them particularly attractive for our application: they can be manufactured in tiny diameters (< 2 mm was demonstrated in [15, 18, 16, 17]), and they have a hollow lumen (i.e. the inner diameter of the tube) which can be used to pass instruments.

As a first step in our investigation, we present a study aiming to establish general kinematic requirements for instrument operation in the larynx. Using three-dimensional anatomical models of the laryngeal cavity, we simulate the insertion and manipulation of steerable instruments with varying degrees of freedom. We define volume and visibility-based metrics to evaluate how well a given design can cover the laryngeal anatomy.

2.1 Kinematic Requirements for Operation Inside the Larynx

Our simulation framework is illustrated in Figure 3. Three-dimensional anatomical models of the larynx were generated based on Computed Tomography (CT) scans of real patients. These models were used as a virtual environment where we simulate the deployment of steerable instruments. In the following sections, we first outline the protocol used to generate the larynx anatomical models and the kinematic model employed to simulate instrument motion. We then describe experimental work aimed to quantify the number of individual degrees of freedom required to maximize an instrument's reach within the larynx.

2.1.1 Three-dimensional Larynx Models

CT scans were selected from the Cancer Genome Atlas Head-Neck Squamous Cell Carcinoma dataset [19], a large multi-institution collection of data regarding patients diagnosed with malignant tumors of the head and neck. To generate a 3D larynx model from a CT scan, we identified the larynx anatomy in the sagittal plane using 3D Slicer (see Figure 3), then we cropped the CT volume to include the tract of the upper airway going from the epiglottis down to the subglottic region (i.e. below the vocal folds), finally we used the segmentation function of 3D slicer to generate a three-dimensional rendering of the cropped volume, which is exported as a stereolithography (STL) model.

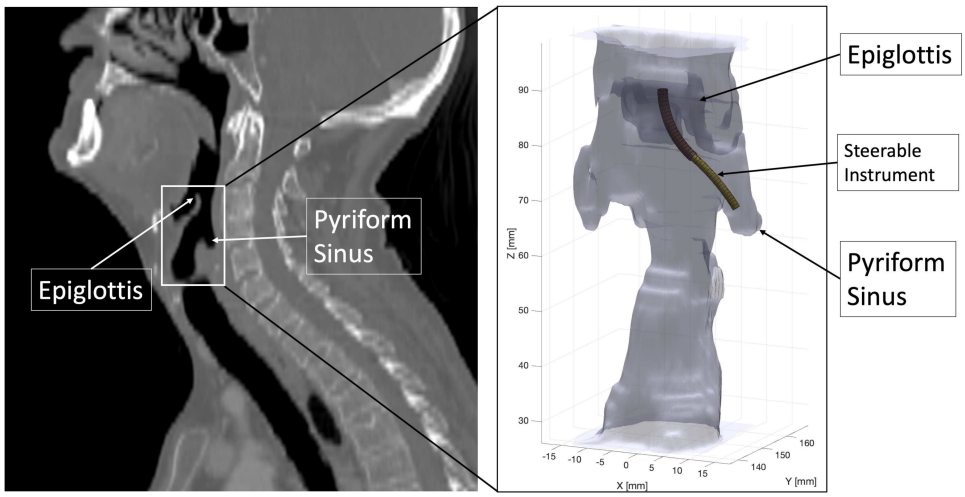

Figure 3: (left) Segmentation of the larynx anatomy in Computed Tomography scans; (right) virtual steerable instrument deployed in a three-dimensional model of the larynx.

2.1.2 Instrument Kinematic Model

The kinematics of continuum bending mechanisms have been extensively investigated in prior work [20]. Assuming no external loading, the shape of these devices can be modeled as a sequence of individual curved links with constant curvature, each characterized by a length ℓ_j, a curvature k_j and an axial rotation ϕ_j (as shown in Figure 4). For a single link, the homogeneous transformation matrix T between the base and the tip, which depends

on tube rotation, length, and curvature, can be calculated using the following product of exponentials:

$$T(k_j, \phi_j, \ell_j) = \mathrm{e}^{\hat{S}_1 \phi_j} \mathrm{e}^{\hat{S}_2 k_j \ell_j} \tag{1}$$

where $S_1 = [0\ 0\ 0\ 0\ 0\ 1]^T$ and $S_2 = [0\ 0\ 1/k_j\ 0\ 1\ 0]^T$. The operator $\hat{}$ that appears in Equation 1 maps twists from $\mathbb{R}^6$ to elements of $\mathfrak{se}(3)$, i.e. the Lie Algebra of the special Euclidean group SE(3). Without loss of generality, we assume that arc parameters k_j, ϕ_j and ℓ_j can be directly controlled. Our framework can be easily extended to account for any mechanism-specific mapping between actuator variables and arc parameters.

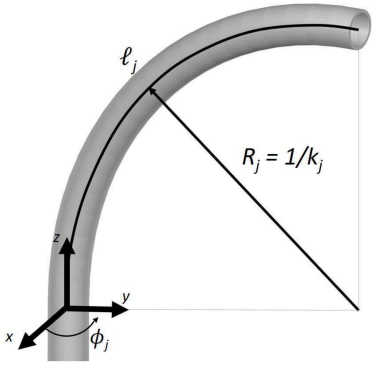

Figure 4: Kinematics of single continuum link

Continuum bending mechanisms can be designed to incorporate an arbitrary sequence of curved links, each having independent degrees of freedom. Intuitively, adding more links will increase the overall dexterity of the mechanism, but will make it more complex to manufacture and control. One question that naturally arises is: how many individual links are necessary for our application? A single curved link may be sufficient to reach any arbitrary point in the larynx (assuming the point falls within actuation limits and that no obstacles are in the way). However, we suspected that adding a second distal link (as shown in Figure 5) might enable more extensive access to tissue. Simulations were conducted to test the deployment of two different instruments, one made of a single steerable link, the second composed of two independently modeled links. Instrument motion was simulated through a sampling-based motion planning algorithm, rapidly-expanding random trees (RRT)[21].

These simulations were performed on five different larynx models.

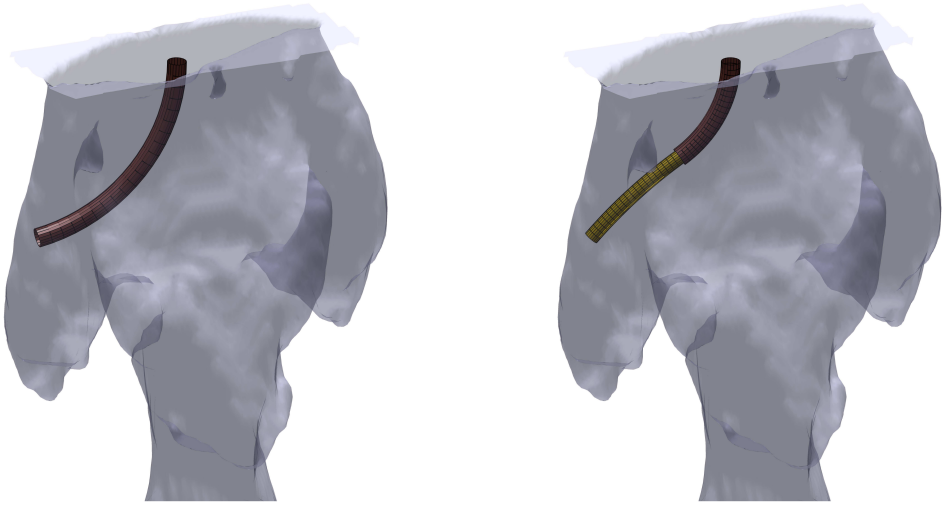

Figure 5: Models of 1-link (left) and 2-link (right) instruments

2.1.3 Volume-Based Metric

The first metric we used to evaluate kinematic models was the total volume of the reachable workspace. RRT was executed to generate a large number of locations (10,000) that can be reached in a collision-free path (see Figure 6). RRT provides probabilistic completeness, meaning the longer the algorithm runs, the more likely it is that it will cover the true reachable volume entirely. Our simulations operated on the arc parameters k_j, ϕ_j and l_j of each individual link, which were left to vary freely within the boundaries specified in Table 1. The MATLAB `boundary` function was used to calculate the tightest single-region boundary around the points generated by RRT, and to estimate its corresponding volume.

Table 1: Range of arc parameters used in simulation

	k_j (mm^{-1})		ϕ_j (rad)		ℓ (mm)	
	min	max	min	max	min	max
One link	0	0.1	0	$2\,\pi$	0	50
Two links	0	0.1	0	$2\,\pi$	0	25

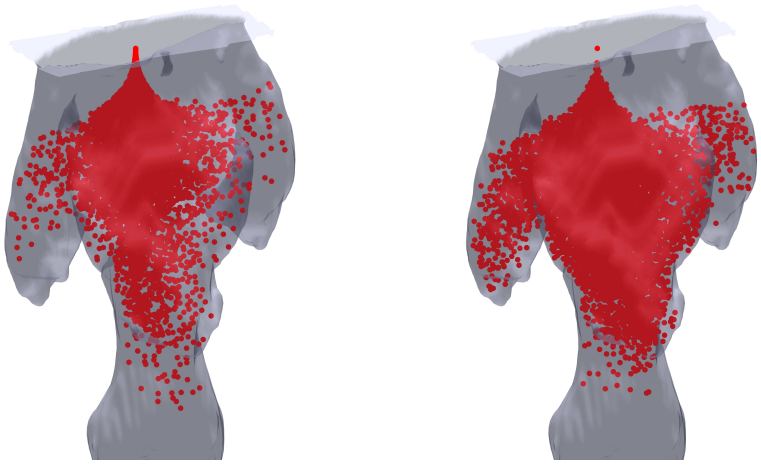

Figure 6: Reachable points with 1-link (left) and 2-link (right) instruments

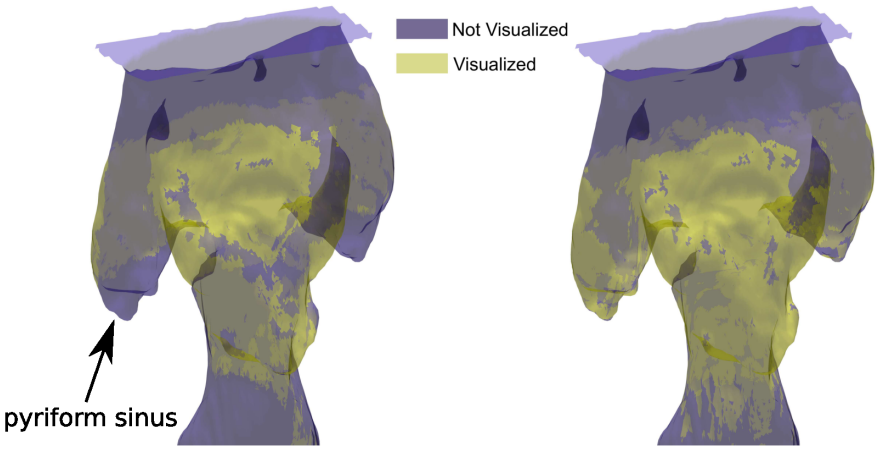

Figure 7: Visible surface with 1-link (left) and 2-link (right) instruments

2.1.4 Visibility-Based Metric

Estimation of visible tissue surface was also performed. This was done by considering the set of reachable points generated by RRT and only selecting those points that were in close proximity to tissue, which was arbitrarily defined as being within a 5mm distance from the internal surface of the larynx. For each of the visible points, we generated visibility maps using the Hidden Point Removal operator [22], combined with a ray-casting procedure that narrowed down visibility within a 20° cone projected from the tip of the instrument. Sample visibility maps calculated with this approach are shown in Figure 7.

Table 2: Results of the volume coverage experiments

Patient ID	One Link (cm^3)	Two Links (cm^3)
1	6.06	5.88
2	6.72	6.96
3	4.32	4.99
4	5.97	7.93
5	8.27	9.04

Table 3: Results of the surface area coverage experiments

Patient ID	One Link (cm^2)	Two Links (cm^2)
1	14.21	20.61
2	19.68	22.55
3	14.10	19.30
4	19.95	25.86
5	19.93	23.34

2.1.5 Simulation Results

Table 2 summarizes the results of the volume estimation procedure. The two-link design was found to provide slightly higher volume coverages in four of the five models. The average difference in volume coverage (absolute value) was found to be 0.76 cm^3. Estimations of reachable surface are reported in Table 3. In all five patients, the two-link design was found to be able to visualize a larger amount of surface area. The average difference in visible surface across the five patients was 4.76 cm^2.

If a tool is needed to work in the pyriform sinuses, the simulations suggest that a two-link design would be required. However, if access to the under-surface of the vocal folds is required, then a one-link design may suffice. In this particular region there is not a notable difference between one-link or two-link manipulators. Due to this result, the decision was made to go with a one-link notched manipulator, as it is simpler to design and manufacture.

2.1.6 Kinematics of Notched Mechanisms

Before describing our simulations for notched mechanisms, we will briefly review their kinematics which were establish by York et al[23]. Each notch can be modeled as a constant curvature link (see Figure 8), with arc parameters: curvature given by Equation 2 and arc length given by Equation 3. The assumption is that when the tendon is pulled, it bends with a constant curvature. The curvature and arc length are plugged into Equation 4, resulting in a transformation matrix for a single notch. For a whole mechanism, this transformation matrix can be propagated. For a more thorough review of notched mechanisms see [23].

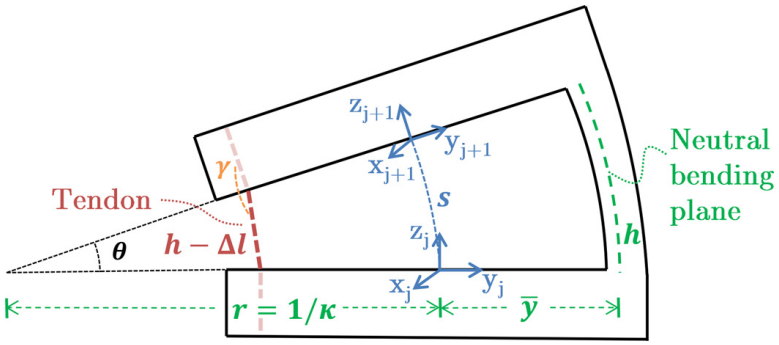

Figure 8: Kinematic overview of a notched mechanism reproduced from [23]

$$\kappa \approx \frac{\Delta l}{h(r_i + \bar{y}) - \Delta l \bar{y}} \tag{2}$$

$$s = \frac{h}{1 + \bar{y}\kappa} \tag{3}$$

$$T = \begin{bmatrix} 1 & 0 & 0 & 0 \\ 0 & cos(\kappa s) & -sin(\kappa s) & (cos(\kappa s) - 1)/\kappa \\ 0 & sin(\kappa s) & cos(\kappa s) & sin(\kappa s)/\kappa \\ 0 & 0 & 0 & 1 \end{bmatrix} \tag{4}$$

2.1.7 Simulations for Developing a Notched Tube

After the decision to go with a notched tube design, it was necessary to determine how many notches were required and their spacing. The simulation framework for determining manipulator type was reconfigured using a model for notched tubes [23]. Simulations were run for four, five, and six notches, each one millimeter deep and one millimeter wide. The simulations were analyzed using the same metrics as the previous simulations: volume coverage and visible surface area. The surface area visible was 17.86, 19.06, and 18.15 square centimeters for four, five, and six notch manipulators respectively. The results of the visible surface area (see Figure 9) showed that four, five, and six notches were effectively the same when accessing the glottic area. Therefore, the decision was made to go with the simplest design, a four notch manipulator. Analyzing the areas reachable and visible through the simulations led to the development of the following requirements: 25 mm of linear advancement, 360 degrees of rotation, and 90 degrees of tip bending.

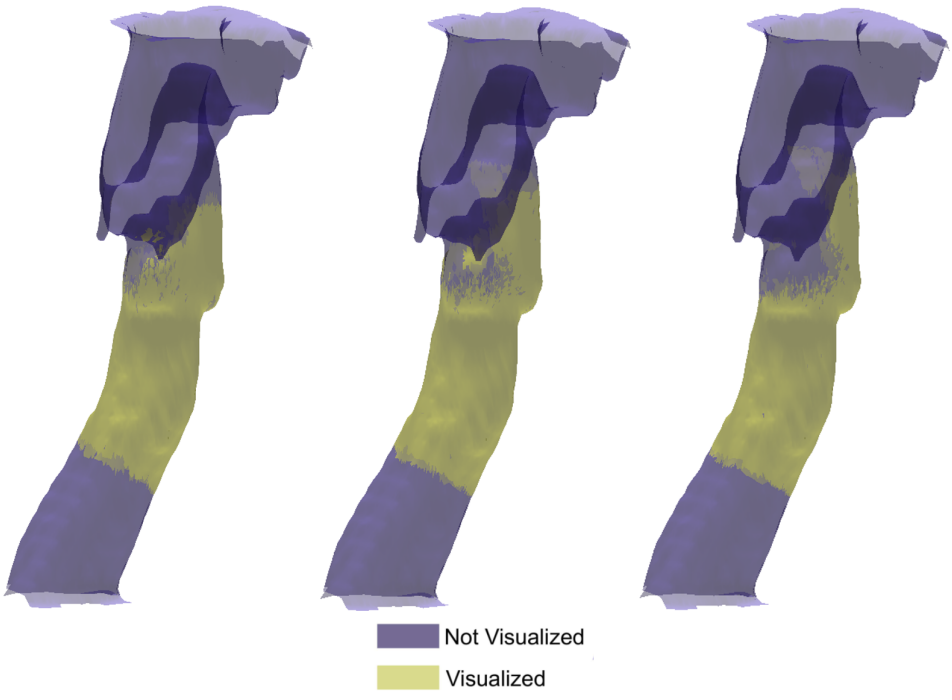

Figure 9: Visible surface with 4-notch (left), 5-notch (middle), 6-notch (right) instruments

2.2 Instrument Design and Fabrication

Based on the kinematic requirements derived in simulation, we developed a platform that consists of three distinct parts: a notched tube end-effector, a flexible shaft, and a transmission, shown below in Figure 10 and Figure 11. An important characteristic of this design is the ability to use multiple tools within our device, such as a laser fiber or small forceps. This created a requirement for a hollow lumen from the transmission through to the end of the notched tube.

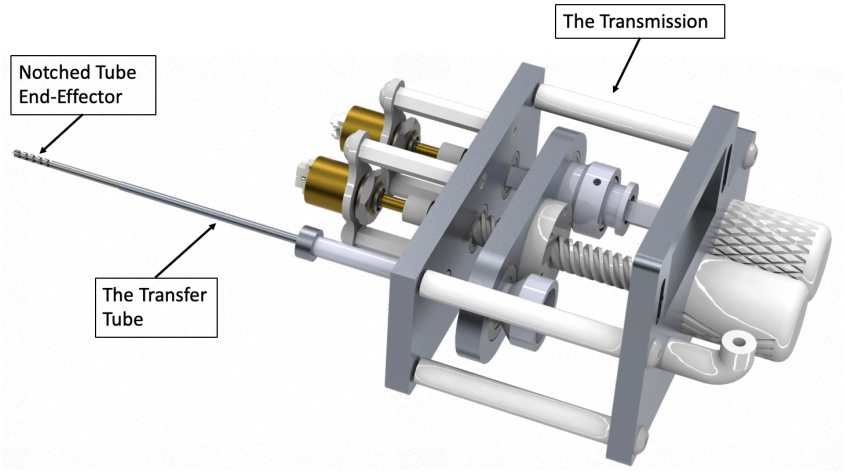

Figure 10: Proposed instrument diagram

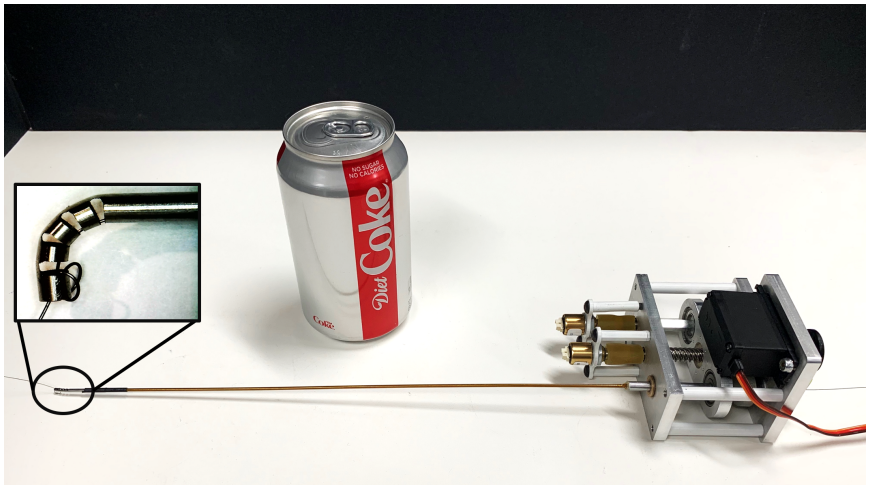

Figure 11: Overview of system

2.2.1 Notched Tube

Regarding the nitinol tube end-effector, we needed to determine an effective way of bending the tube. While nitinol is super-elastic, the wall thickness of the tube is so small compared to its outer diameter that it cannot bend 90 degrees without breaking. To resolve this, we cut relief notches in the tube that were evenly spaced and at a consistent depth enabling the tube to bend without exceeding its elastic deformation range. We developed a fabrication process that consisted of grinding the nitinol notches instead of milling them. We created a fixture, as shown in Figure 12, to mount the grinding wheel into a milling machine and cut the notches in the tube. While we improved the machining process, the removal of the nitinol from its fixture was still a challenge because the nitinol would snap. Our solution was to make the fixture into two pieces that separated upon completion of the cutting process.

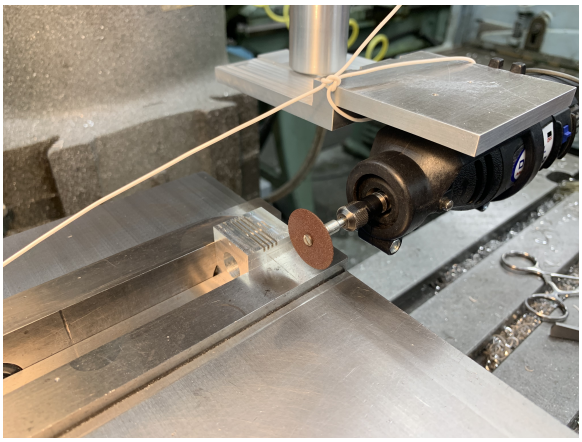

Figure 12: Machining setup in milling machine

The end product was a notched nitinol tube (1.8 mm outer diameter) that could bend to the designed angle as predicted by our simulations. It was articulated by a nitinol wire that was super glued to the end notch. This is shown below in Figure 13.

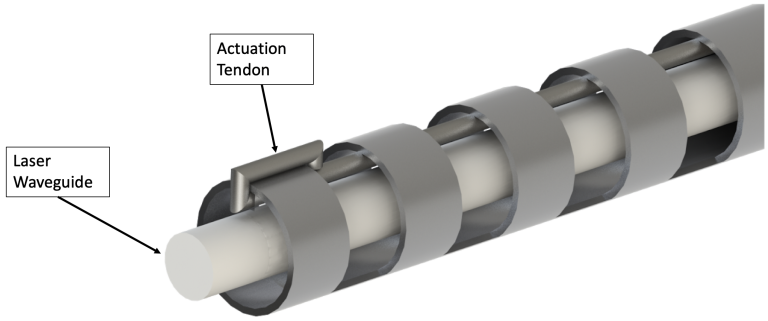

Figure 13: Single link, notched lumen for waveguide deployment

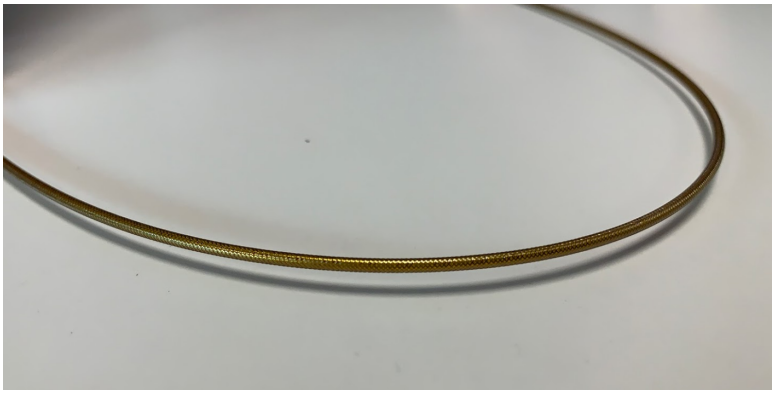

Figure 14: Braided nitinol tubing

2.2.2 Flexible Shaft

Our solution required a hollow, flexible shaft that could transmit rotation and translation. Our first concept was to use a nitinol tube similar to that of the notched tube. While the nitinol would transmit the necessary rotation and translation, it was not compliant enough to follow the curved working channel of the endoscope without breaking. Therefore, we determined that a super-elastic tube was still necessary, but further research needed to be completed to develop a compliant enough design. Our next solution was a plastic tube that was braided with nitinol wire as shown in Figure 14. Specifically, we utilized MicroLumen's Polyimide Tubing code 630.

This tube was able to transmit the necessary rotation and translation like the nitinol tubing, but was flexible enough to bend down the working channel of the scope. The next step was to determine how the flexible shaft would connect to both the transmission output

shaft and the notched tube. We needed the flexible shaft to be rigidly attached to both so that it would transmit the necessary rotation and translation while deployed in the scope. After first testing with retaining compounds, such as super glue, we determined that heat shrink was the best way to attach the components together for the prototype as it was rigid enough to transmit the rotation and translation (see Figure15).

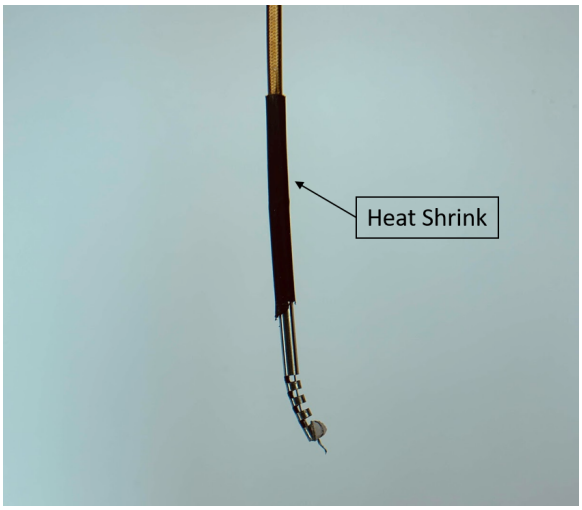

Figure 15: Heat shrink connection between notched tube and flexible shaft

2.2.3 Transmission

We developed a small transmission module that provides our notched tube instrument with three degrees of freedom inside the larynx based on designs of similar instrumentation. Inspiration for the transmission came from a recent research article from Hendrick et al. [24]. The design featured in the article used a combination of a leadscrew, linear bearing, and square shaft to deliver translation and rotation to the end effector. We adapted the design of [24] to meet the motion requirements of the end effector developed from our simulations: translation of 25 mm, rotation through 360 degrees, and up to 90 degrees of bending. A full rendering of our design is shown in Figure 16.

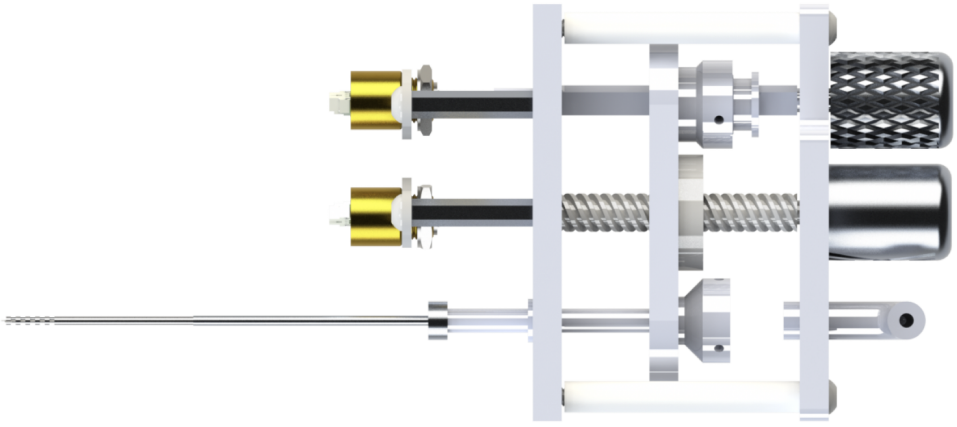

Figure 16: Top-down device rendering

The structure of the transmission is focused around three aluminum plates that provide mounting and support for other components in the transmission. We chose to make these plates from aluminum rather than 3D printed materials because aluminum offered several distinct advantages. First, by pressing the bearings into the plates, which cannot be accomplished with 3D printed materials, we simplified the design significantly. Further simplification was possible because strong threads can be created in aluminum which allowed us to remove additional components from the assembly. Figure 17 defines the various plates within the assembly. Plate C provides a surface to mount the transmission's two sensors on plastic plates stood off from Plate C. Plate A provides the mounting surface for the user

controls and a servo module, which is used to bend the tip of the notched tube. Plates A and C are connected by four bolts, each running through a plastic standoff. Plate B differs from Plates A and C in that it is not rigidly mounted and is designed to translate between Plates A and C.

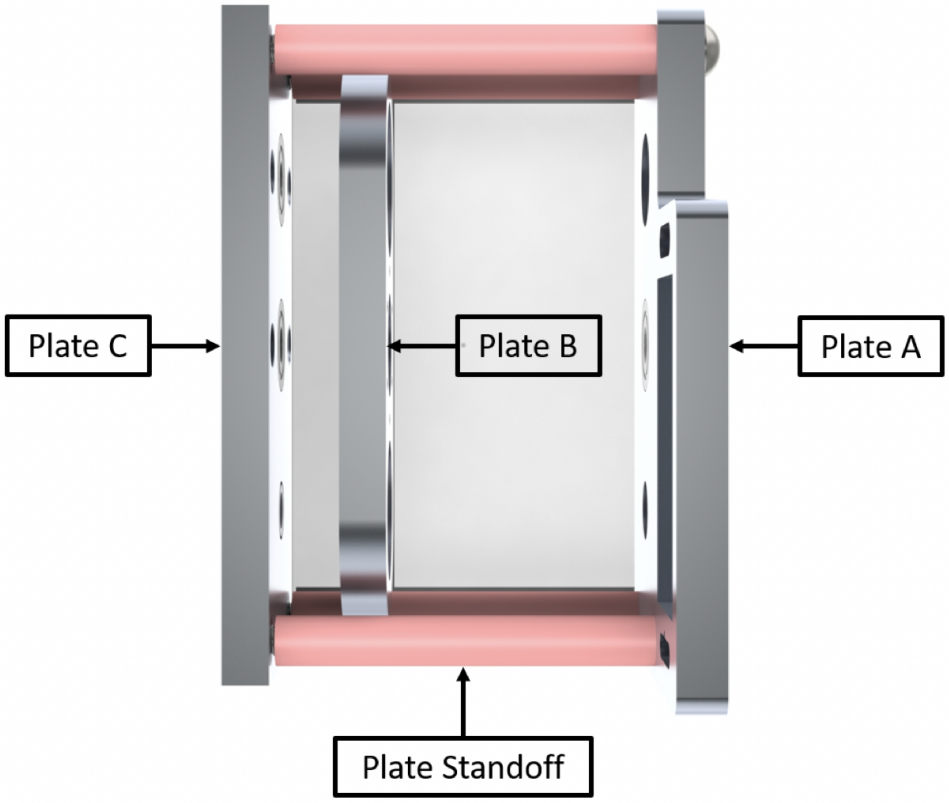

Figure 17: Annotated top-down view of plate structure in transmission

The controls of the transmission are simple, but clearly differentiated, to allow the user to operate the transmission without looking back at the controls. Two knobs are located on Plate A which were 3D printed to allow a knurled texture to be applied. The knob for translation features a half knurled texture while the knob for rotation features a fully knurled texture as shown in Figure 18.

The translation of the flexible shaft is achieved through the use of a leadscrew to allow exact analog control. The translational components are outlined in Figure 19. The leadscrew is mounted to shielded ball bearings on Plates A and C and is rigidly connected to the user control knob and absolute encoder. The leadscrew nut is rigidly connected to Plate B which

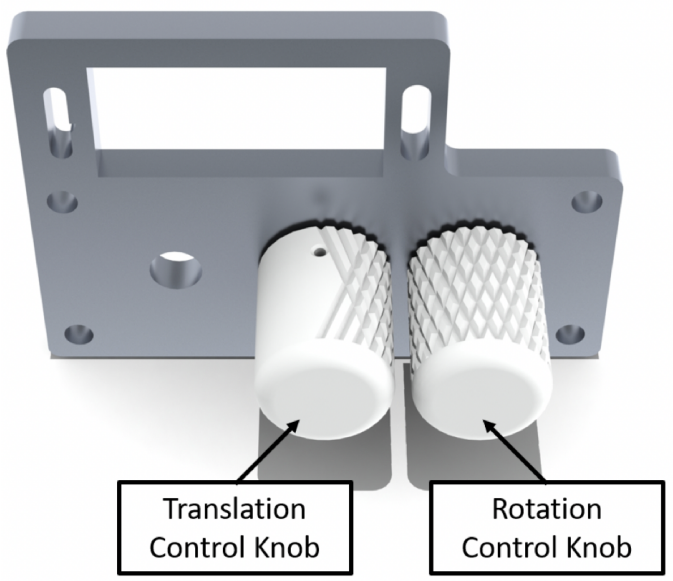

Figure 18: Annotated front view of control knobs

prevents the nut from rotating and forces the nut to translate linearly. The output shaft of the transmission is then attached to the middle plate which allows the output shaft to translate with Plate B. The leadscrew is an ultra precision leadscrew (McMaster part no. 2391N24) with minimized backlash to give the user more exact and repeatable control.

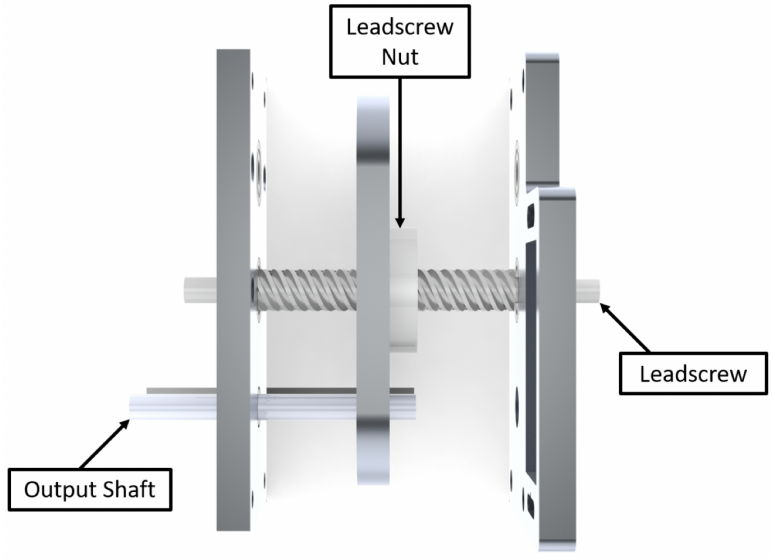

Figure 19: Annotated top-down view of translation components

The rotation of the flexible shaft was designed to give the user exact control without complicated mechanical linkages. The components necessary for rotation are outlined in Figure 20. This mechanism uses a square shaft and a linear bearing that rides along said shaft. The bearing transfers the rotation of the shaft without being affected by its own translation along the shaft. This bearing is also connected to Plate B via a shielded ball bearing, which allows it to rotate, and to the output shaft via a belt and pulley system. This belt and pulley system is responsible for transferring the rotation of the square shaft to the output shaft. Both the absolute encoder and user control are connected directly to the square shaft. However, at these connections, we turned the square shaft to be round. These circular portions serve a double purpose of reducing the cost of the overall product and reducing the complexity of the mechanism. Round bearings are more readily available than square bearings which allowed us to buy off the shelf products. The transition from square to round shaft also created a retaining feature that retained the shaft between the two plates without using additional hardware. This square shaft serves a secondary purpose of preventing Plate B from rotating.

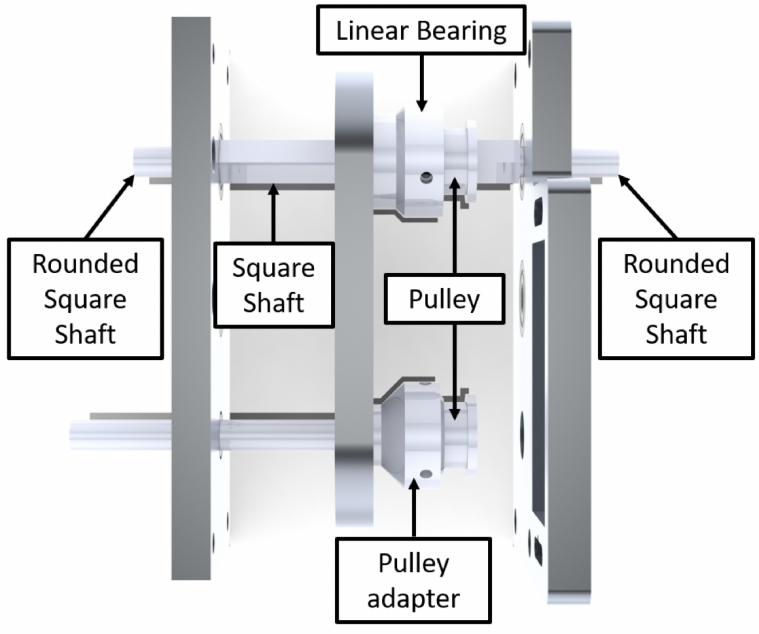

Figure 20: Annotated top-down view of rotation components

The actuation of the notched tube with a servo module provides precise control while stationary and while translating. The nitinol wire used to bend the notched tube passes into the transmission through the center of the hollow output shaft shown in Figure 21. This allows the string to pass through the transmission without interfering with the other mechanisms. The wire then passes through Plate A and turns 90 degrees upwards to wrap around a pulley on the mounted servo. By pulling the nitinol wire, the servo can bend the tip and adjust the length of the wire based on the extension of the notched tube in the larynx. Ultimately, the servo was required to pull approximately 27 mm of wire, 25 mm for the translation of the tool and 2 mm for the bending of the tool.

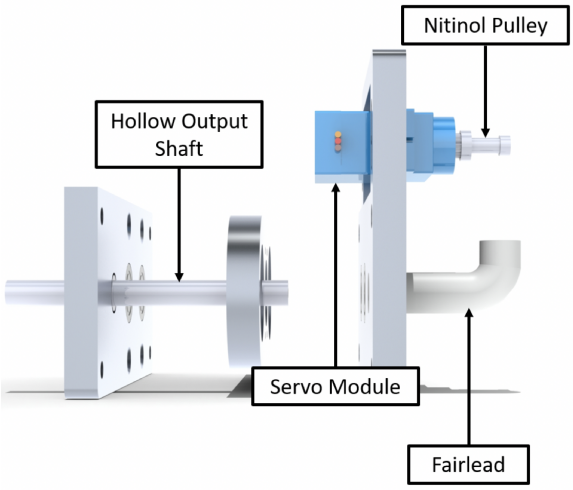

Figure 21: Annotated side-view of tip displacement components

A prototype of this transmission module, as seen in Figure 22, was realized and tested. Manufacturing of this transmission proved to be manageable and did not necessitate any major redesigns.

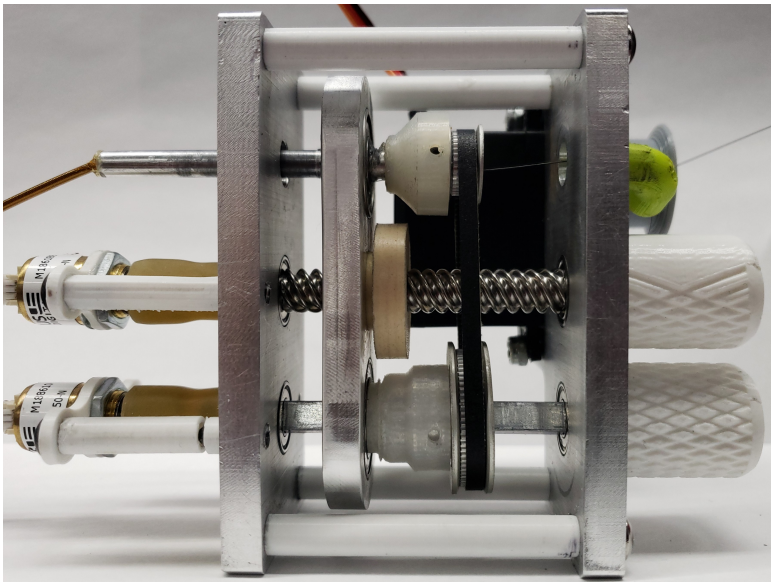

Figure 22: Bottom-up view of assembled transmission module

2.3 Incorporating Sensing/Visualization

Thinking towards the actual implementation of this device in an operative setting, we determined that a live, digital visualization of the tool may be helpful to understand the position of the flexible mechanism during operation, as the surgeon may not be able to accurately visualize the tool. Furthermore, this visualization allows for improved testing, research, and feedback during operation. This tool was developed not only to give a visual indication of the manipulator's state, but also to give warning when the tool is at its maximum rotation, displacement, or advancement. The design included sensors to measure the positioning of the various methods of manipulation. An MA3 absolute encoder (US Digital, Vancouver, WA) was mounted on the shaft and leadscrew for rotation and advancement respectively. These encoders are analog, and wraparound after one revolution. The positioning of the servo for displacement was also used for input to the visualization.

Our visualization allowed the use of any device with WiFi and a screen. Initial testing of the concept involved streaming sensor data to a computer using an ESP8266. The benefit of this device is that it is affordable (<$10), has built-in WiFi, and is supported by the standard Arduino libraries and IDE. This was switched to an ESP32 as that device supports more than

one analog input and also features Bluetooth. The ESP32 is still quite affordable (<$20). Data from both absolute encoders was streamed to a client device using a WebSocket over ESP32 WiFi.

Data from the ESP32 is received by a web browser that provides a graphical visualization of the current orientation of the notched manipulator. The kinematic model for the manipulator was developed by York et. al [23]. This model was implemented in JavaScript and runs in the browser based upon the sensor data received from the ESP32. The output of the model is then visualized using the p5.js open source visualization library [25]. This library creates a canvas that allows for the creation of cylinders for the base length of the tube and the advancement. A 3D-model of a notch segment is added to the canvas for the visualization of each notch as seen in Figure 23.

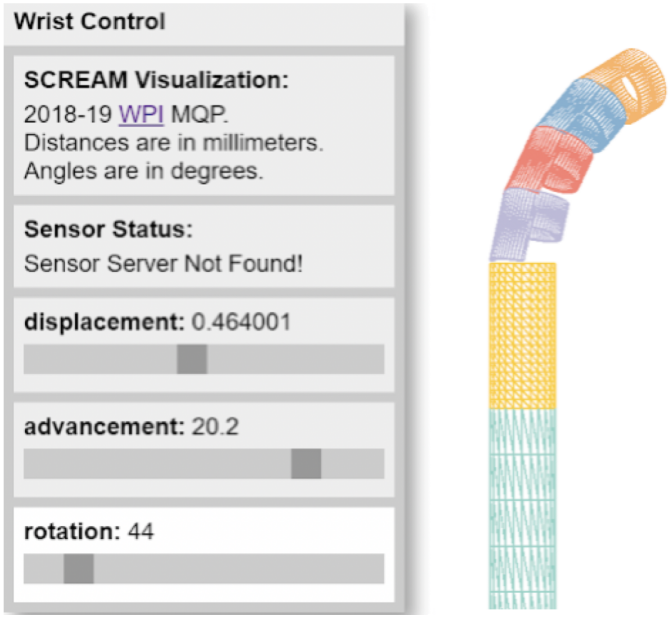

Figure 23: Visualization of notched tube

3 Testing and Validation

3.1 Benchmark Verification

After developing the device, we needed to test the capabilities of the prototype. The three metrics that we identified for best verifying these capabilities were testing the advancement, the rotation, and the distal bending of the end effector. The test showed that the advancement measured about 23mm, shown in Figure 24.

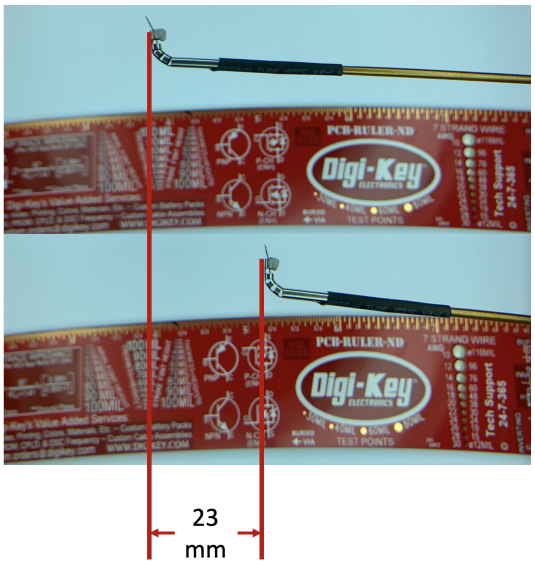

Figure 24: Linear advancement of the device by 23 mm

While we were aiming for 25mm of advancement, we believe that the device was within tolerance for our purposes and the difference was due to manufacturing tolerances. Our desired rotation was 360 degrees and our device achieved greater than 360 degrees of rotation. The end effector rotated 180 degrees is shown below in Figure 25.

Our testing showed that continually rotating the device would cause the actuation tendon inside to coil and snap the notched tube. By limiting the device to only 360 degrees of rotation in one direction, we eliminated the risk of snapping the notched tube. The distal bending goal for our device was 90 degrees utilizing the servo and pull wire method shown in Figure 26.

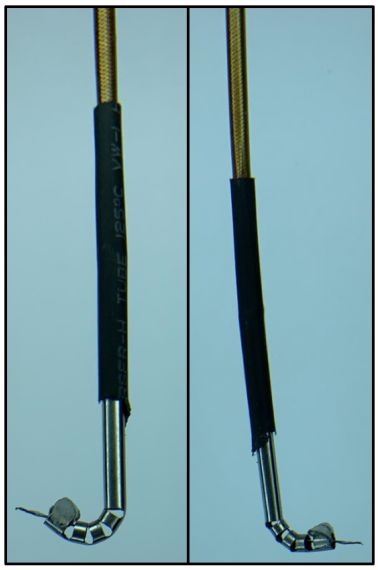

Figure 25: Rotation of notched tube by 180 degrees

Figure 26: Bending of notched tube by 90 degrees

From testing, we determined that our device could articulate past our 90 degree goal; however, we also found that after increased and continued displacement, the nitinol would slightly fatigue and no longer return to its original and unbent form. This state is shown in the left side of Figure 26. We also tested linking the servo and the encoder monitoring the linear advancement together so that the distal bending angle would remain constant while the notched tube translated through the larynx.

3.2 In Vitro Verification

To test that the platform could actually reach the anatomy we originally described, we 3D printed a singular model of the larynx based upon the same CT scans used in the simulations detailed above at a 1:1 scale. Once printed, we were able to pass our device into the model and verify that our tool not only achieved equivalent metrics to current medical devices, but also that it could go beyond. The figure below shows our tool's ability to reach a lesion on the underside of the vocal folds, an area previously unreachable to current devices.

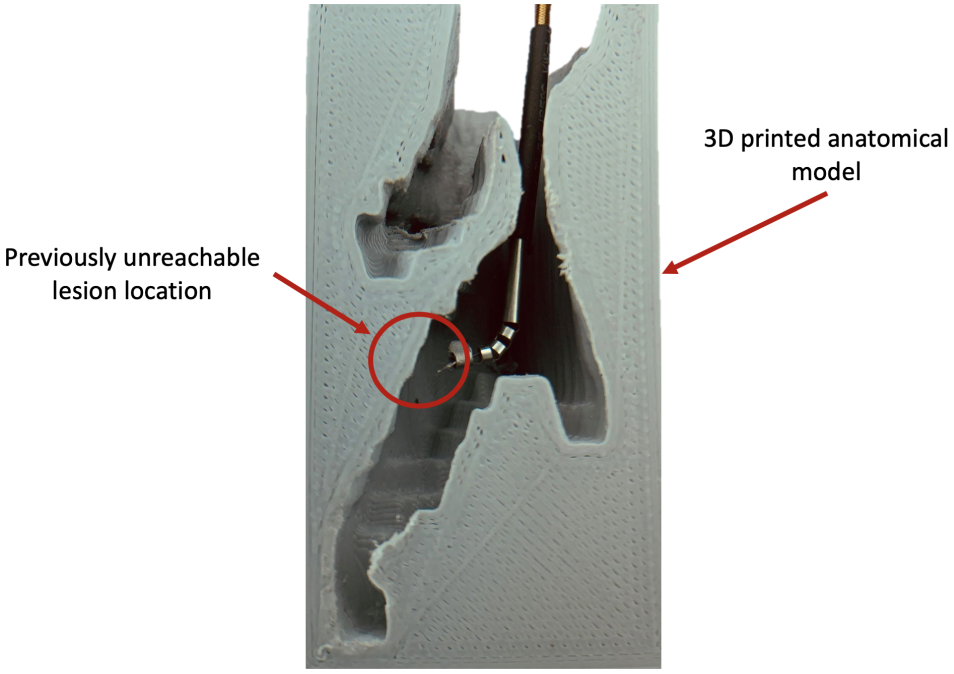

Figure 27: In vitro verification of device

4 Discussion and Future Work

From the work completed by this team, several areas of further work have been noted that would improve the current design of the system and aid in developing a more automated and integrated process.

4.1 Notched Tube

The notched tube for bending at the tip proved to be a successful solution to the problem of articulation. An extension to this project could explore notched tubes on multiple sides to develop a flexible tube from nitinol that could replace the braided catheter flexible shaft. This could potentially be better for transmitting the necessary torque and translation while down the endoscope. Another potential extension would be exploring different notch patterns on the nitinol to create specialty tools to reach specific areas in the larynx. These new end effectors could carry different tools other than the laser with which we worked.

4.2 Flexible Shaft

The plastic tube braided with nitinol proved to be an effective solution to the problem that our flexible shaft faced, as it could transmit the necessary torque and translation. We believe, however, that future work can investigate better methods of attaching the flexible shaft to the transmission and to the notched tube. Our solution to this was specifically for testing and would not be suitable in a sterile environment. The solution would need to be sturdy enough to transmit the necessary forces, but also be sterile enough to be used in a medical environment.

4.3 Transmission

The transmission module was proven to successfully complete all of the design requirements but lacks many of the ergonomic considerations seen in other commercial medical devices. The current device is a large rectangular prism that is hard to hold in one hand. Compounding this problem is that the controls are not in a place where they can easily be manipulated if holding the device in one hand.

Future development of the device should seek to remedy these issues by rearranging the location of components within the transmission and developing a complete outer shell that would encompass all of the components of the assembly. These changes should be done in a close working partnership with the personnel who would use the device. Their input would allow the most important functions be placed in easy reach with effective controls.

4.4 Visualization

More warnings that are integrated with the visualization would be useful. One identified area is warnings regarding degraded laser power due to bending. It is anticipated that the bending of the notched tube will lead to decreased power output as the laser is bent. A warning system could provide the operator with notifications to increase the laser output

power. More warnings could be added to indicate the end of manipulator travel as well.

Another benefit could be integrating the instrument visualization with a scan of the patient for real-time tracking. This would allow the physician to understand exactly where in the patient the manipulator is. Procedures could be planned ahead of time, which could allow for a faster and more accurate procedure.

After the development of a motor-controlled flexible manipulator, it could be possible to automate its operation and remove human error from the procedure. Before full automation, aids to the physician can be developed. The literature currently suggests that augmented reality could provide assistance with many medical applications, including polyp detection [26]. It is understood that polyps are missed because they are never in the field of view or they were in the field of view but not recognized. Overall, augmented reality and further automation could expand beyond the added features of a flexible manipulator.

References

[1] J Hun Hah, Songyong Sim, Soo-Youn An, Myung-Whun Sung, and Hyo Geun Choi. Evaluation of the prevalence of and factors associated with laryngeal diseases among the general population. *The Laryngoscope*, 125(11):2536–2542, 2015.

[2] Wolfgang Steiner, Petra Ambrosch, and Ulrich Braun. *Endoscopic laser surgery of the upper aerodigestive tract: with special emphasis on cancer surgery*, volume 1. Thieme Stuttgart, 2000.

[3] David J Wellenstein, Henrieke W Schutte, Robert P Takes, Jimmie Honings, Henri AM Marres, James A Burns, and Guido B van den Broek. Office-based procedures for the diagnosis and treatment of laryngeal pathology. *Journal of Voice*, 32(4):502–513, 2018.

[4] Catherine J Rees, Gregory N Postma, and Jamie A Koufman. Cost savings of unsedated office-based laser surgery for laryngeal papillomas. *Annals of Otology, Rhinology & Laryngology*, 116(1):45–48, 2007.

[5] Alexander T Hillel, Matthew C Ochsner, Michael M Johns III, and Adam M Klein. A cost and time analysis of laryngology procedures in the endoscopy suite versus the operating room. *The Laryngoscope*, 126(6):1385–1389, 2016.

[6] Anthony G Del Signore, Rupali N Shah, Nikita Gupta, Kenneth W Altman, and Peak Woo. Complications and failures of office-based endoscopic angiolytic laser surgery treatment. *Journal of Voice*, 30(6):744–750, 2016.

[7] Hao-Chun Hu, Shu-Yi Lin, Yi-Ting Hung, and Shyue-Yih Chang. Feasibility and associated limitations of office-based laryngeal surgery using carbon dioxide lasers. *JAMA Otolaryngology–Head & Neck Surgery*, 143(5):485–491, 2017.

[8] Soo Min Hwang, Doh Young Lee, Nu-Ri Im, Hyun-Ji Lee, Byoungjae Kim, Kwang-Yoon Jung, Tae Hoon Kim, and Seung-Kuk Baek. Office-based laser surgery for benign

laryngeal lesion. *Medical Lasers; Engineering, Basic Research, and Clinical Application*, 4(2):65–69, 2015.

[9] Marc Hamoir, Juliette Fievez, Sandra Schmitz, Dorris Velasco, and Benoît Lengele. Extended voice-sparing surgery in selected pyriform sinus carcinoma: Techniques and outcomes. *Head & neck*, 35(10):1482–1489, 2013.

[10] What is recurrent respiratory papillomatosis?, 2004.

[11] deSilva B. Pan Q. Matrka L. Ivancic R., Iqbal H. Current and future management of recurrent respiratory papillomatosis. *Laryngoscope investigative otolaryngology*, 3(1):22–34, 2018.

[12] Recurrent respiratory papillomatosis, 2016.

[13] Gottlieb SL Markowitz LE Chesson HW, Forhan SE. The potential health and economic benefits of preventing recurrent respiratory papillomatosis through quadrivalent human papillomavirus vaccination. *Vaccine*, 26(35):4513–4518, 2008.

[14] Filip Jelínek, Ewout A Arkenbout, Paul WJ Henselmans, Rob Pessers, and Paul Breedveld. Classification of joints used in steerable instruments for minimally invasive surgerya review of the state of the art. *Journal of Medical Devices*, 9(1):010801, 2015.

[15] Philip J Swaney, Peter A York, Hunter B Gilbert, Jessica Burgner-Kahrs, and Robert J Webster. Design, fabrication, and testing of a needle-sized wrist for surgical instruments. *Journal of medical devices*, 11(1):014501, 2017.

[16] P Francis, KW Eastwood, V Bodani, T Looi, and JM Drake. Design, modelling and teleoperation of a 2 mm diameter compliant instrument for the da vinci platform. *Annals of biomedical engineering*, pages 1–13, 2018.

[17] Margaret Rox, Katherine Riojas, Maxwell Emerson, Kaitlin Oliver-Butler, D Caleb Rucker, and Robert James Webster. Luminal robots small enough to fit through endoscope ports: initial tumor resection experiments in the airways. In *Proceedings of the Hamlyn Symposium on Medical Robotics 2018*, pages 63–64, 2018.

[18] Loris Fichera, Neal P Dillon, Dongqing Zhang, Isuru S Godage, Michael A Siebold, Bryan I Hartley, Jack H Noble, Paul T Russell, Robert F Labadie, and Robert J Webster. Through the eustachian tube and beyond: A new miniature robotic endoscope to see into the middle ear. *IEEE robotics and automation letters*, 2(3):1488–1494, 2017.

[19] ML Zuley, R Jarosz, S Kirk, Y Lee, R Colen, K Garcia, and ND Aredes. Radiology data from the cancer genome atlas head-neck squamous cell carcinoma [tcga-hnsc] collection, 2017.

[20] Robert J Webster and Bryan A Jones. Design and kinematic modeling of constant curvature continuum robots: A review. *The International Journal of Robotics Research*, 29(13):1661–1683, 2010.

[21] S.M. LaValle. *Planning Algorithms*. Cambridge University Press, 2006.

[22] Sagi Katz, Ayellet Tal, and Ronen Basri. Direct visibility of point sets. In *ACM SIGGRAPH 2007 Papers*, SIGGRAPH '07, New York, NY, USA, 2007. ACM.

[23] Peter A York, Philip J Swaney, Hunter B Gilbert, and Robert J Webster. A wrist for needle-sized surgical robots. In *2015 IEEE International Conference on Robotics and Automation (ICRA)*, pages 1776–1781. IEEE, 2015.

[24] Richard J Hendrick, Christopher R Mitchell, S Duke Herrell, and Robert J Webster III. Hand-held transendoscopic robotic manipulators: A transurethral laser prostate surgery case study. *The International journal of robotics research*, 34(13):1559–1572, 2015.

[25] Processing. processing/p5.js, Apr 2019.

[26] Nadim Mahmud, Jonah Cohen, Kleovoulos Tsourides, and Tyler M Berzin. Computer vision and augmented reality in gastrointestinal endoscopy. *Gastroenterology report*, 3(3):179–184, 2015.